Wake structure and thrust generation of a flapping foil in two-dimensional flow

A. Andersen[1,†], **T. Bohr**[1], **T. Schnipper**[1,2,‡] **and J. H. Walther**[2,3]

[1]Department of Physics and Center for Fluid Dynamics, Technical University of Denmark, DK-2800 Kgs. Lyngby, Denmark

[2]Department of Mechanical Engineering and Center for Fluid Dynamics, Technical University of Denmark, DK-2800 Kgs. Lyngby, Denmark

[3]Swiss Federal Institute of Technology Zürich, Chair of Computational Science, ETH Zentrum, Clausiusstrasse 33, CH-8092 Zürich, Switzerland

We present a combined numerical (particle vortex method) and experimental (soap film tunnel) study of a symmetric foil undergoing prescribed oscillations in a two-dimensional free stream. We explore pure pitching and pure heaving, and contrast these two generic types of kinematics. We compare measurements and simulations when the foil is forced with pitching oscillations, and we find a close correspondence between flow visualisations using thickness variations in the soap film and the numerically determined vortex structures. Numerically, we determine wake maps spanned by oscillation frequency and amplitude, and we find qualitatively similar maps for pitching and heaving. We determine the drag–thrust transition for both pitching and heaving numerically, and we discuss it in relation to changes in wake structure. For heaving with low oscillation frequency and high amplitude, we find that the drag–thrust transition occurs in a parameter region with wakes in which two vortex pairs are formed per oscillation period, in contrast to the common transition scenario in regions with inverted von Kármán wakes.

Key words: propulsion, vortex shedding, wakes/jets

1. Introduction

Oscillating foils can lead to the formation of a variety of spectacular vortex patterns (Koochesfahani 1986, 1989; Schnipper *et al.* 2010), and such flows and the forces that generate them are at the same time of great significance in fluid–structure interactions, e.g. for understanding the function of swimming appendages in biological

† Email address for correspondence: aanders@fysik.dtu.dk
‡ Present address: Svend Ole Hansen ApS, Sct. Jørgens Allé 5 C, DK-1615 Copenhagen, Denmark.

A. Andersen, T. Bohr, T. Schnipper and J. H. Walther

locomotion (Lighthill 1969; Triantafyllou, Triantafyllou & Yue 2000). The kinematics and dynamics of swimming appendages in nature are typically complex, involving a combination of pitching and heaving (Sfakiotakis, Lane & Davies 1999), effects of foil flexibility (Marais *et al.* 2012; Jaworski & Gordnier 2015), and three-dimensional flows (Buchholz & Smits 2008).

In the present paper, we consider a rigid foil with prescribed flapping motion in a two-dimensional free stream to explore basic aspects of wake formation and the associated fluid forces. Experimentally and numerically, we consider two generic types of kinematics, pure pitching and pure heaving respectively. We used a gravity-driven vertically flowing soap film for our experimental study (Rutgers, Wu & Daniel 2001), and the experimental set-up and main observations were first presented by Schnipper, Andersen & Bohr (2009). Our simulations of two-dimensional incompressible Newtonian flow were carried out using a particle vortex method (Walther & Larsen 1997), and the numerical findings have not been presented previously. The round leading edge and the wedge-shaped trailing edge of the symmetric foil give rise to two distinct sources of vorticity, i.e. the boundary layers along the two sides of the foil and the trailing edge, leading to the formation of simple or complex vortex wakes depending on the oscillation frequency and amplitude.

Soap film tunnels have been used as simple and powerful flow visualisation tools for a variety of vortex flows (Couder & Basdevant 1986; Gharib & Derango 1989; Rivera, Vorobieff & Ecke 1998; Zhang *et al.* 2000), but only a few studies have explored to what extent soap film flows provide a quantitative analogy with two-dimensional incompressible Newtonian flows (Couder, Chomaz & Rabaud 1989; Chomaz & Cathalau 1990). We therefore explore the relation between the vortex structures visualised experimentally using thickness variations in the quasi-two-dimensional soap film flows and the vortex structures in the corresponding two-dimensional incompressible Newtonian flows obtained numerically.

Further, we contrast the wake formation in the two kinematic modes using the numerical simulations, and we consider the net fluid forces on the flapping foil, with particular focus on the drag–thrust transition and its relation to changes in wake structure. This problem has been investigated previously for pure pitching motion in experiments in which the drag–thrust transition was inferred from flow field measurements (Godoy-Diana, Aider & Wesfreid 2008; Bohl & Koochesfahani 2009), in direct measurements using force transducers (Mackowski & Williamson 2015) and in numerical simulations (Das, Shukla & Govardhan 2016). We add to these studies by comparing the drag–thrust transition in the two different kinematic modes under similar flow conditions, and we find an atypical transition scenario for the heaving foil at low oscillation frequency and high amplitude.

2. Foil kinematics and dimensionless parameters

The foil is rigid and has a semicircular leading edge with diameter D, chord length C, aspect ratio $D/C = 1/6$ and straight sides that form a wedge-shaped trailing edge (Schnipper *et al.* 2009). The foil is placed in a uniform inflow with speed U in the x-direction, and it is oscillated with frequency f and amplitude A. In the pure pitching mode (figure 1*a*), the foil pitches around the centre of the semicircular leading edge such that the foil angle ϕ with respect to the free-stream direction varies with the simple harmonic motion
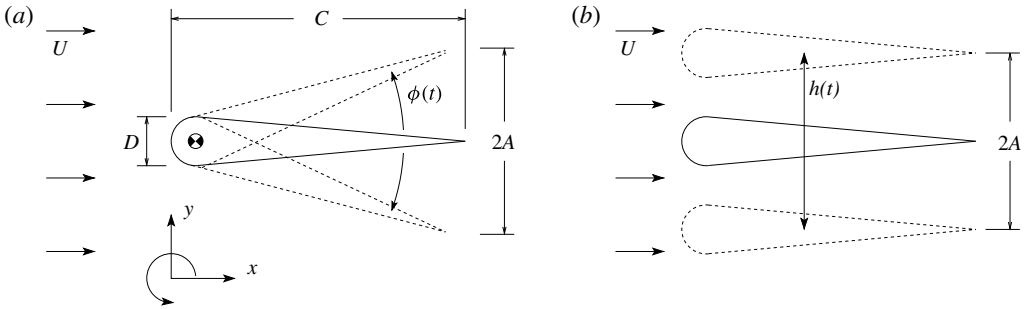
$$\phi(t) = \phi_0 \sin 2\pi f t, \tag{2.1}$$

FIGURE 1. Geometry and kinematics of the foil. (*a*) Pure pitching and (*b*) pure heaving.

where the amplitudes ϕ_0 and A are connected by the relation $\sin \phi_0 = 12A/(11C)$. In the pure heaving mode (figure 1*b*), the foil oscillates transversely to the free stream such that the *y*-coordinate of the centreline of the foil h follows the equation

$$h(t) = A \sin 2\pi ft. \tag{2.2}$$

The oscillating foil in the two-dimensional incompressible Newtonian flow is characterised by three dimensionless parameters, i.e. the width-based Strouhal number

$$St_D = \frac{Df}{U}, \tag{2.3}$$

the dimensionless amplitude

$$A_D = \frac{2A}{D} \tag{2.4}$$

and the Reynolds number based on the chord length $Re = CU/\nu$, where ν is the kinematic viscosity of the fluid. The width-based Strouhal number St_D describes the externally imposed frequency and not the natural vortex shedding frequency, and it is sometimes referred to as the Keulegan–Carpenter number. The product of St_D and A_D is the so-called amplitude-based Strouhal number,

$$St_A = \frac{2Af}{U}. \tag{2.5}$$

The amplitude-based Strouhal number can be understood as the ratio between the speed of the foil tip and the speed of the free stream, and it plays a central role in describing the drag–thrust transition (Triantafyllou, Triantafyllou & Gopalkrishnan 1991).

3. Particle vortex method

The numerical simulations were performed using a two-dimensional discrete particle vortex method. The approach is described in detail elsewhere (Walther & Larsen 1997; Rasmussen *et al.* 2010), and it has been validated for the flow past a flat plate (Walther & Larsen 1997; Hejlesen *et al.* 2015) and for the flow past suspension-bridge sections (Larsen & Walther 1997). The method is based on a Lagrangian formulation of the two-dimensional vorticity equation

$$\frac{\partial \omega}{\partial t} + (\boldsymbol{v} \cdot \boldsymbol{\nabla}) \omega = \nu \nabla^2 \omega, \tag{3.1}$$

where $\boldsymbol{v}$ denotes the velocity and $\boldsymbol{\omega} = \nabla \times \boldsymbol{v}$ the vorticity. At each time step, the instantaneous fluid velocity is obtained from the Biot–Savart relation

$$
\begin{aligned}
\boldsymbol{v}(x, y) = \boldsymbol{U} &+ \frac{1}{2\pi} \iint_{S_{fluid}} \frac{\boldsymbol{\omega}(x', y') \times (\boldsymbol{x} - \boldsymbol{x}')}{|\boldsymbol{x} - \boldsymbol{x}'|^2} \, \mathrm{d}x' \, \mathrm{d}y' \\
&- \frac{1}{2\pi} \oint_{C_{foil}} \frac{[\boldsymbol{v}(x', y') \cdot \boldsymbol{n}(x', y')](\boldsymbol{x} - \boldsymbol{x}') - [\boldsymbol{v}(x', y') \times \boldsymbol{n}(x', y')] \times (\boldsymbol{x} - \boldsymbol{x}')}{|\boldsymbol{x} - \boldsymbol{x}'|^2} \, \mathrm{d}l',
\end{aligned}
\tag{3.2}
$$

where $\boldsymbol{n}$ denotes the outward unit normal at the foil boundary, C_{foil} the foil boundary and S_{fluid} the fluid domain. The boundary integral accounts for the vorticity within the foil due to the solid-body rotation. The foil boundary is discretised using boundary elements with vortex sheets of linearly varying strength. In the present study, we discretise the foil boundary using 400 elements and conduct the simulations for 10 periods of the flapping motion. The no-slip boundary condition is imposed by solving a boundary integral equation obtained from (3.2) for the unknown vortex sheet strengths while satisfying Kelvin's circulation theorem. The vortex sheets are subsequently diffused into the flow to form the no-slip boundary layer. The advection is described by the inviscid motion of the discrete vortex particles, and viscous diffusion is modelled using the method of random walks (Chorin 1973). In the simulations, we have $Re = 2640$ to match the experiments (Schnipper *et al.* 2009). To reduce computational costs, the velocity equation (3.2) is computed using the adaptive fast multipole method (Carrier, Greengard & Rokhlin 1988), and vortex particles are amalgamated five chord lengths downstream of the trailing edge. Control simulations without amalgamation show that amalgamation has no effect on the fluid forces acting on the foil.

The instantaneous net fluid force on the foil is computed from the equation

$$
\boldsymbol{F}(t) = \rho \frac{\mathrm{d}}{\mathrm{d}t} \left(\iint_{S_{foil}} \boldsymbol{v} \, \mathrm{d}x \, \mathrm{d}y - \iint_{S_{fluid}} \boldsymbol{x} \times \boldsymbol{\omega} \, \mathrm{d}x \, \mathrm{d}y \right),
\tag{3.3}
$$

where ρ is the density of the fluid and S_{foil} is the domain occupied by the foil (Wu 1981; Walther & Larsen 1997). We shall, for convenience, decompose the net fluid force on the foil into thrust and lift components $F_T = -F_x$ and $F_L = F_y$, and use the standard definitions of the instantaneous thrust and lift coefficients

$$
C_T = \frac{F_T}{(1/2)\rho C U^2}, \quad C_L = \frac{F_L}{(1/2)\rho C U^2}.
\tag{3.4a,b}
$$

From (3.3), we obtain the equation for the thrust component

$$
F_T = -\rho \frac{\mathrm{d}}{\mathrm{d}t} \left(\iint_{S_{foil}} v_x \, \mathrm{d}x \, \mathrm{d}y - \iint_{S_{fluid}} y\omega \, \mathrm{d}x \, \mathrm{d}y \right).
\tag{3.5}
$$

The equation highlights the close connection between the transition from drag to thrust and the transition in the arrangement of the coherent vortices in the wake, e.g. from von Kármán wake with y and ω predominantly of opposite signs to inverted von Kármán wake with y and ω predominantly of the same sign (von Kármán & Burgers 1935).
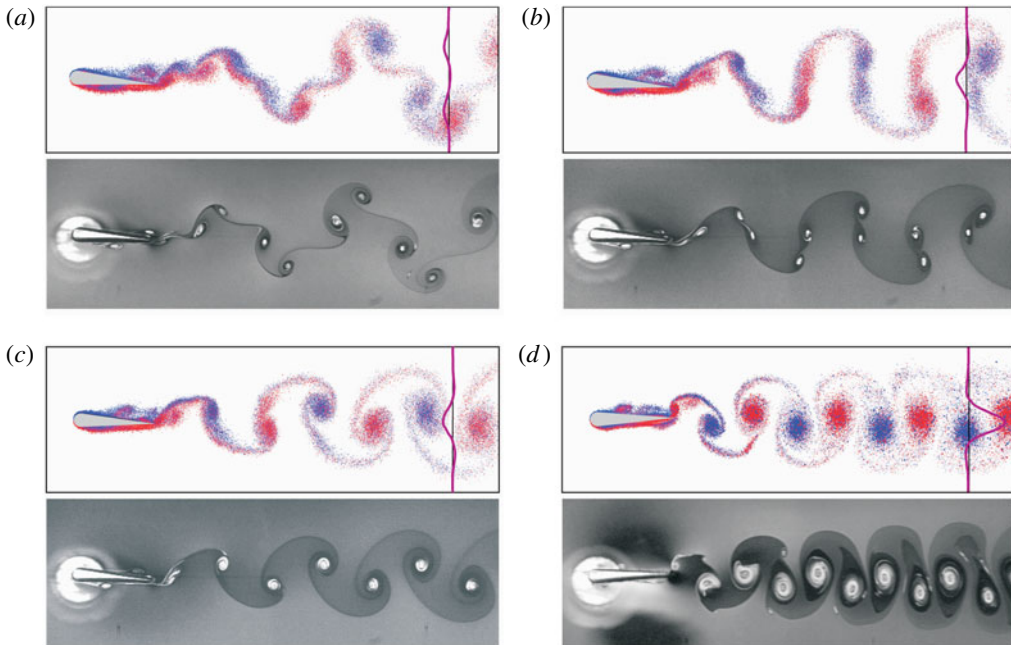
FIGURE 2. Wakes of the pitching foil in simulation (colour) and experiment (greyscale). Red (blue) corresponds to positive (negative) vorticity, and the magenta lines show average velocity profiles four chord lengths downstream of the trailing edge, with the black lines showing the inflow velocity as reference. (*a*) A 2P wake ($St_D = 0.08$, $A_D = 1.14$ and $\langle C_T \rangle = -0.12$), see also supplementary movie 1 available at https://doi.org/10.1017/jfm.2016.808; (*b*) a 2P wake that evolves to a von Kármán wake ($St_D = 0.11$, $A_D = 1.14$ and $\langle C_T \rangle = -0.12$); (*c*) a von Kármán wake ($St_D = 0.12$, $A_D = 1.14$ and $\langle C_T \rangle = -0.12$); (*d*) an inverted von Kármán wake ($St_D = 0.18$, $A_D = 1.65$ and $\langle C_T \rangle = 0.00$).

4. Pitching foil in experiment and simulation

We first consider the pitching foil in experiment and simulation. We shall label the wakes using the symbols introduced by Williamson & Roshko (1988), where $mS + nP$ signifies m single vortices and n vortex pairs shed per oscillation period. Figure 2 shows a 2P wake (*a*), a 2P wake that evolves downstream to a von Kármán wake (*b*), a von Kármán wake (*c*) and an inverted von Kármán wake (*d*). In the simulation images, each dot corresponds to a vortex particle with positive (red) or negative (blue) circulation. Regions with high dot density that are dominated by red (blue) dots correspond to vortices of positive (negative) net circulation. The wake types are identified by visual inspection in the approximate interval 2–4 chord lengths downstream of the trailing edge, and the soap film experiment additionally allows us to use a long 20 chord length interval to follow the downstream wake evolution.

In all four cases, we observe that the vortex particles in the simulation and the thickness variations in the soap film form similar structures, i.e. concentrated vortices connected by narrow curved bands of vorticity. Agreement is also observed in the flow close to the leading and trailing edges, where four patches of vorticity form in every oscillation period. For example, both methods show the formation of two vortex patches, one on each side of the leading edge, per flapping period. After formation, the patches roll downstream along the foil (Schnipper *et al.* 2009). In figure 2(*b*), we plot
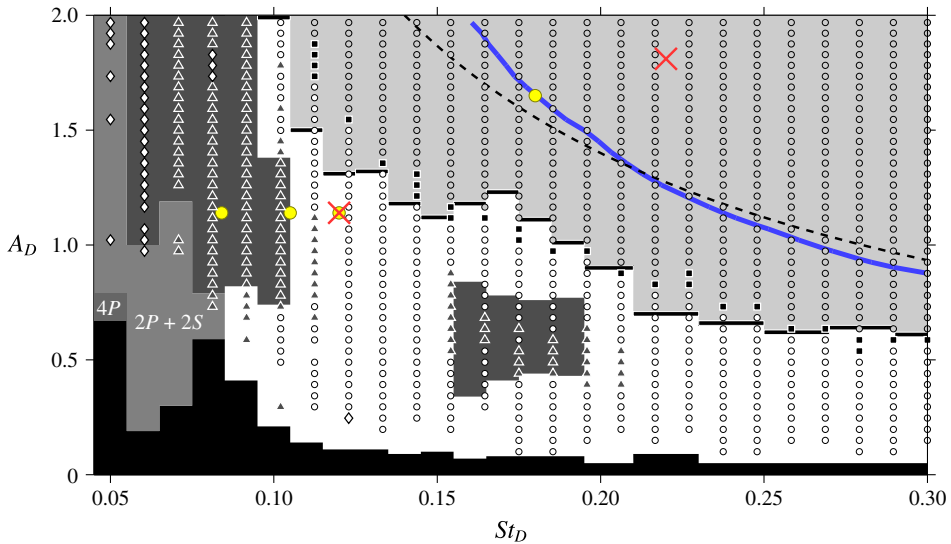
FIGURE 3. Wake map for the pitching foil. Experiment (background shades) and simulation (symbols): ($\bigcirc$, white) von Kármán wakes, ($\bullet$, light grey) inverted von Kármán wakes, ($\blacksquare$, black bars) aligned $2S$ wakes with vortices on the symmetry line, ($\triangle$, dark grey) $2P$ wakes and ($\diamondsuit$) periodic vortex wakes with blurry vorticity regions. The yellow discs indicate the cases in figure 2 and the red crosses the examples shown in figure 4. The solid blue curve shows the drag–thrust transition and the dashed black curve shows the contour line with $St_A = 0.28$.

an intermediate wake type in which a $2P$ wake evolves downstream to a von Kármán wake by pairwise merging of vortices. We note that a slight decrease of St_D yields a stable $2P$ wake, whereas a slight increase yields a von Kármán wake. Differences between simulation and experiment are also observed: the vortices in the inverted von Kármán wake in figure 2(d) are located 18 % closer to each other in the experiment than in the simulation. We presume that this is due to the relatively intense flapping of the foil, which gives rise to compressibility effects in the soap film flow (Chomaz & Cathalau 1990).

The four wakes in figure 2 are representative of the most significant wake types in the wake map (phase diagram) in figure 3. The symbols indicating periodic wake types in the simulation are plotted on top of the corresponding wake map (shaded areas) measured in the soap film (Schnipper *et al.* 2009). Wakes with no clear periodicity were found in the simulations where symbols are absent in the phase diagram, and in the soap film where the background shade is black. Generally, there is a striking overall agreement in the variety of vortex wakes. Both methods find a region ($St_D > 0.1$) that is dominated by $2S$ wake types, as observed by Godoy-Diana *et al.* (2008), and a region ($St_D < 0.1$) that is dominated by complex wakes. We observe that the numerical and experimental boundaries between the von Kármán wake and the inverted von Kármán wake correspond well with each other, and only at low frequencies and high amplitudes do we find some quantitative differences. The simulations also reproduce two non-overlapping regions with the $2P$ wake measured in the soap film, i.e. one main region and a small island embedded in the von Kármán region. The $2P$ wakes occur as vortices formed at the leading and trailing edges are shed in turn with a spatial separation sufficiently large to prevent the vortices from
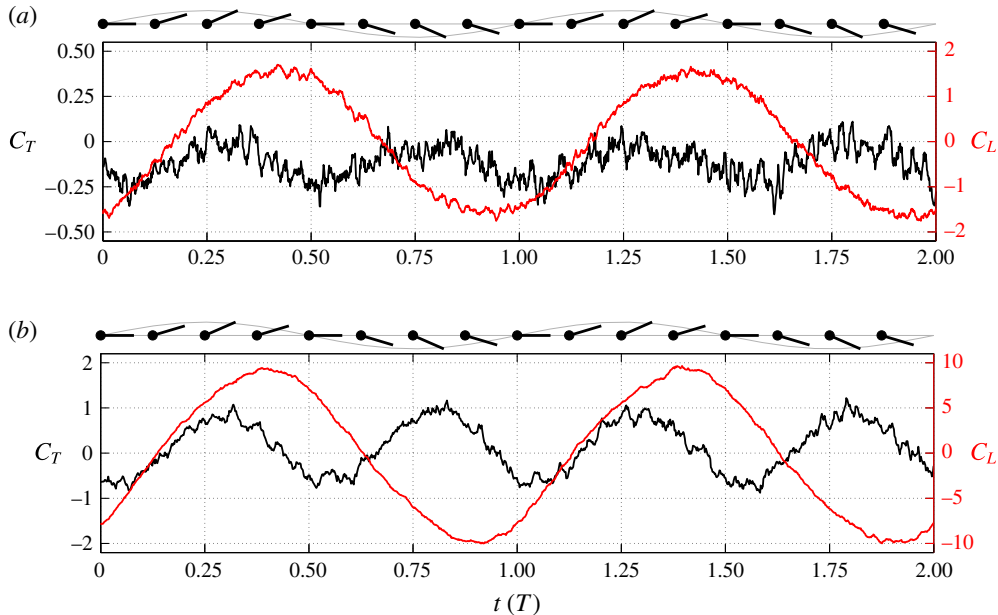
FIGURE 4. Instantaneous thrust (black) and lift (red) coefficients for the pitching foil in the simulation. (*a*) von Kármán wake (cf. figure 2*c*) with average drag ($St_D = 0.12$ and $A_D = 1.14$) and (*b*) inverted von Kármán wake with average thrust ($St_D = 0.22$ and $A_D = 1.81$).

merging (Schnipper *et al.* 2009). From animations of the flow fields, it is confirmed that the same process takes place in the simulations. These observations indicate that the boundary layer evolutions in the simulation and in the soap film agree well. The agreement in the horizontal width of the 2*P* island furthermore shows that the spatial threshold for vortex merging is the same in the two methods (Schnipper *et al.* 2009).

Figure 4 shows the instantaneous thrust and lift for the pitching foil in two representative examples: (*a*) $St_D = 0.12$ and $A_D = 1.14$, giving rise to a von Kármán wake and average drag $\langle C_T \rangle = -0.12$, and (*b*) $St_D = 0.22$ and $A_D = 1.81$, giving rise to an inverted von Kármán wake and average thrust $\langle C_T \rangle = 0.18$. The simulation noise is due to the random walks of the vortex particles (Chorin 1973), and the curves are obtained by applying a 10-point moving average filter to the raw numerical data. The instantaneous lift varies periodically with the period *T* of the foil motion, and the instantaneous drag varies periodically with half of the period, as expected from the reflection symmetry in the problem. Average thrust is only produced by the pitching foil when it is oscillated with sufficiently high frequency and amplitude to give rise to an inverted von Kármán wake (figure 3). More precisely, the drag–thrust transition (solid blue curve) takes place at $St_A = 0.28$ (dashed black curve), which is a higher value than the transition between von Kármán wake and inverted von Kármán wake at $St_A = 0.18$ (Schnipper *et al.* 2009). This observation is in agreement with previous measurements and simulations (Godoy-Diana *et al.* 2008; Bohl & Koochesfahani 2009; Das *et al.* 2016), whereas inviscid theory predicts a drag–thrust transition as the wake changes from von Kármán wake to inverted von Kármán wake (von Kármán & Burgers 1935).
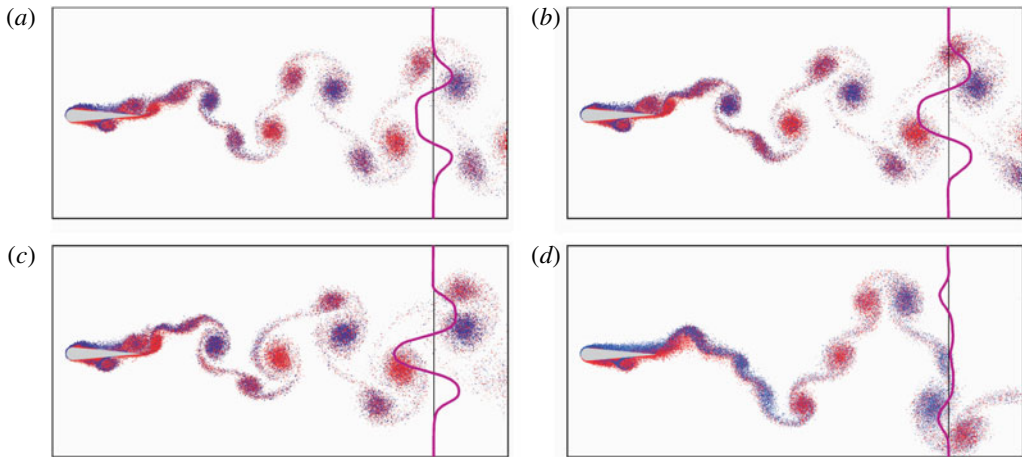
FIGURE 5. Selected wakes of the heaving foil in simulation. Red (blue) corresponds to positive (negative) vorticity, and the magenta lines show average velocity profiles four chord lengths downstream of the trailing edge, with the black lines showing the inflow velocity as reference. (*a*) A $2P$ wake with average drag ($St_D = 0.10$, $A_D = 1.40$ and $\langle C_T \rangle = -0.03$); (*b*) a $2P$ wake immediately below the drag–thrust transition ($St_D = 0.10$, $A_D = 1.60$ and $\langle C_T \rangle = -0.01$); (*c*) a $2P$ wake with average thrust ($St_D = 0.10$, $A_D = 1.80$ and $\langle C_T \rangle = 0.02$), see also supplementary movie 2; (*d*) a $2P + 2S$ wake ($St_D = 0.06$, $A_D = 1.60$ and $\langle C_T \rangle = -0.09$).

5. Heaving foil in simulation

The heaving foil forms a variety of $2P$ wakes (figure 5). For increasing A_D, the vortex pairs point still more downstream, indicating an increasing amount of thrust production. Figure 5(*a*) is, in fact, a case where the foil experiences average drag, figure 5(*b*) is a case immediately below the drag–thrust transition and figure 5(*c*) is a case of average thrust production. In addition, figure 5(*d*) shows a $2P + 2S$ wake where six vortices are shed in each flapping period. A similar wake type is found, for quite similar flapping parameters, behind the pitching foil in the soap film (figure 3). However, the two $2P + 2S$ wakes differ qualitatively in the sense of rotation of the vortex closest to the centreline. The heaving foil sheds three same-signed vortices per flapping half-period. In contrast, the pitching foil, cf. figure 3(*d*) in Schnipper *et al.* (2009), forms wake arrangements with vortices of alternating sense of rotation.

Similarly to the pitching foil, the wake map for the heaving foil consists of a region ($St_D > 0.1$) dominated by $2S$ wake types and a region ($St_D < 0.1$) that is dominated by more complex wake types (figure 6). Further, it can be noticed that two non-overlapping regions of $2P$ wake exist in the wake map: a main region that is located at $0.06 < St_D < 0.12$ and a small island at $0.19 < St_D < 0.23$ embedded in the von Kármán wake region. The formation of vortex patches close to the leading and trailing edges appears to be similar to the pitching foil. From animations of the flow field, we measure that a leading-edge vortex rolls downstream along the chord with velocity $0.64U$. Following the simple model by Schnipper *et al.* (2009), we obtain the theoretical estimates $St_D = 0.11$ for the centre of the main $2P$ region and $St_D = 0.22$ for the centre of the $2P$ island, in reasonably good agreement with the wake map based on the numerical simulations.
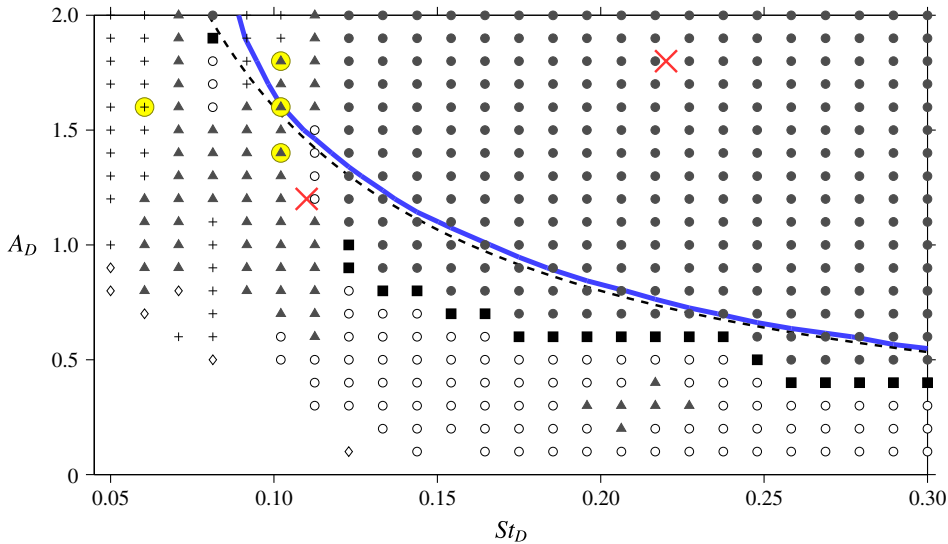
FIGURE 6. Wake map for the heaving foil in simulation: (+) $2P + 2S$ wakes, (◯) von Kármán wakes, (●) inverted von Kármán wakes, (■) aligned $2S$ wakes, (▲) $2P$ wakes and (◇) periodic vortex wakes with blurry vorticity regions. The yellow discs indicate the cases in figure 5 and the red crosses the examples shown in figure 7. The solid blue curve shows the drag–thrust transition and the dashed black curve shows the contour line with $St_A = 0.16$.

For the heaving foil, the transition from von Kármán wake to inverted von Kármán wake takes place at lower amplitudes than for the pitching foil (figures 3 and 6). In the upper-right part of the wake map, we find oblique inverted von Kármán wakes (Marais *et al.* 2012; Das *et al.* 2016). In the region $St_D < 0.12$, the wake map has a complex structure. In addition to $2P$ wakes, we observe exotic $2P + 2S$ wakes, somewhat scattered in the region. In contrast to the case of the pitching foil, we find a transition from $2P$ wake to inverted von Kármán wake by increasing St_D for constant amplitude in the range $1.5 < A_D \leqslant 2.0$. We do not observe systematically any von Kármán wake to inverted von Kármán wake transition in this region.

Figure 7 shows the instantaneous thrust and lift for the heaving foil in two representative examples: (*a*) $St_D = 0.11$ and $A_D = 1.20$, giving rise to a von Kármán wake and average drag $\langle C_T \rangle = -0.03$, and (*b*) $St_D = 0.22$ and $A_D = 1.80$, giving rise to an inverted von Kármán wake and average thrust $\langle C_T \rangle = 0.39$. We observe both $2P$ and $2P + 2S$ in the thrust region of the heaving foil (figure 6), and we see that an indication of average thrust production is that the vortex pairs in the $2P$ wake point in the downstream direction (figure 5*c*). The vortex pairs give rise to average jet flow above and below the symmetry line, in contrast to the inverted von Kármán wake with strong average jet flow on the symmetry line (figure 2*d*). Similarly to the pitching foil, we observe that the drag–thrust transition (solid blue curve) closely follows an St_A contour line, albeit at the lower value $St_A = 0.16$ (dashed black line). We note that $2P$ wakes with average thrust, interpreted from slices through three-dimensional vortex rings, have been measured behind freely swimming fish such as bluegill sunfish (Drucker & Lauder 2002) and eel (Tytell & Lauder 2004).
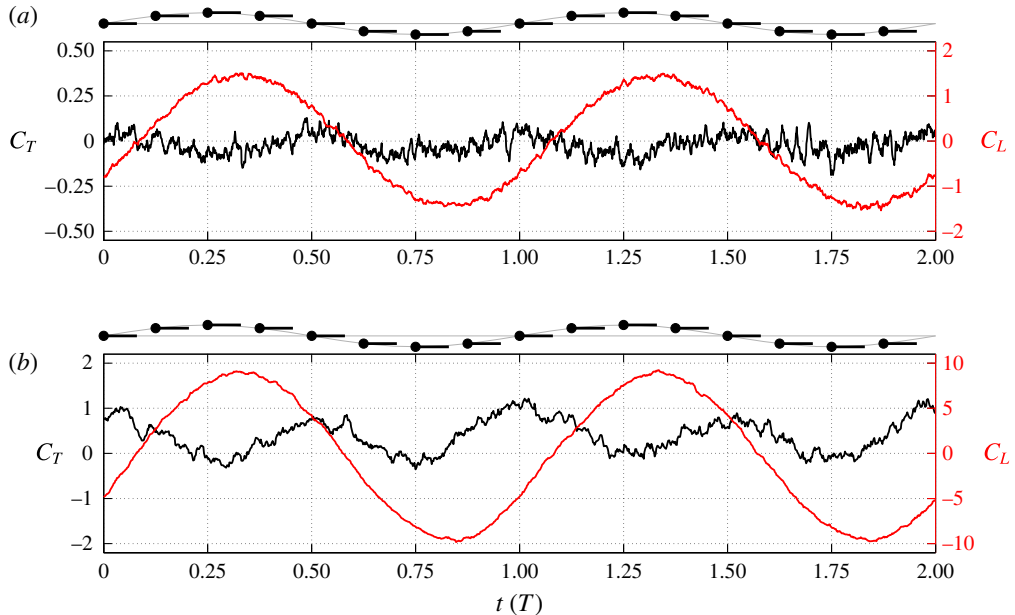
A. Andersen, T. Bohr, T. Schnipper and J. H. Walther

FIGURE 7. Instantaneous thrust (black) and lift (red) coefficients for the heaving foil in simulation. (*a*) von Kármán wake with average drag ($St_D = 0.11$ and $A_D = 1.20$) and (*b*) inverted von Kármán wake with average thrust ($St_D = 0.22$ and $A_D = 1.80$).

It will be interesting to explore to what extent the results of the present study are applicable to three-dimensional situations.

6. Conclusions

The agreement between the vortex particle method and the measurements in the soap film tunnel shows that the soap film technique is a versatile tool to visualise flow structures and to relate them to the corresponding two-dimensional incompressible Newtonian flows. Only at high oscillation frequency and amplitude did we observe differences, presumably due to the compressibility of the soap film. The wake maps summarising the wake types for pitching and heaving turned out to be qualitatively similar. The main difference in the wake structures and thrust production between the two different kinematic modes turned out to be the relation between the drag–thrust transition and the changes in wake structure at low oscillation frequency and high amplitude, where the heaving foil displayed drag–thrust transition in a 2*P* wake region with jets symmetrically above and below the symmetry line.

Acknowledgements

Supplementary movies

Supplementary movies are available at https://doi.org/10.1017/jfm.2016.808.

References

BOHL, D. G. & KOOCHESFAHANI, M. M. 2009 MTV measurements of the vortical field in the wake of an airfoil oscillating at high reduced frequency. *J. Fluid Mech.* **620**, 63–88.

BUCHHOLZ, J. H. J. & SMITS, A. J. 2008 The wake structure and thrust performance of a rigid low-aspect-rato pitching panel. *J. Fluid Mech.* **603**, 331–365.

CARRIER, J., GREENGARD, L. & ROKHLIN, V. 1988 A fast adaptive multipole algorithm for particle simulations. *SIAM J. Sci. Stat. Comput.* **9** (4), 669–686.

CHOMAZ, J.-M. & CATHALAU, B. 1990 Soap films as two-dimensional classical fluids. *Phys. Rev.* A **41**, 2243–2245.

CHORIN, A. J. 1973 Numerical study of slightly viscous flow. *J. Fluid Mech.* **57** (4), 785–796.

COUDER, Y. & BASDEVANT, C. 1986 Experimental and numerical study of vortex couples in two-dimensional flows. *J. Fluid Mech.* **173**, 225–251.

COUDER, Y., CHOMAZ, J. M. & RABAUD, M. 1989 On the hydrodynamics of soap films. *Physica* D **37**, 384–405.

DAS, A., SHUKLA, R. K. & GOVARDHAN, R. N. 2016 Existence of a sharp transition in the peak propulsive efficiency of a low-*Re* pitching foil. *J. Fluid Mech.* **800**, 307–326.

DRUCKER, E. G. & LAUDER, G. V. 2002 Experimental hydrodynamics of fish locomotion: functional insights from wake visualization. *Intl Comput. Biol.* **42**, 243–257.

GHARIB, M. & DERANGO, P. 1989 A liquid film (soap film) tunnel to study two-dimensional laminar and turbulent shear flows. *Physica* D **37**, 406–416.

GODOY-DIANA, R., AIDER, J.-L. & WESFREID, J. E. 2008 Transitions in the wake of a flapping foil. *Phys. Rev.* E **77**, 016308.

HEJLESEN, M. M., KOUMOUTSAKOS, P., LEONARD, A. & WALTHER, J. H. 2015 Iterative Brinkman penalization for remeshed vortex methods. *J. Comput. Phys.* **280**, 547–562.

JAWORSKI, J. W. & GORDNIER, R. 2015 Thrust augmentation of flapping airfoils in low Reynolds number flow using a flexible membrane. *J. Fluids Struct.* **52**, 199–209.

VON KÁRMÁN, T. & BURGERS, J. M. 1935 General aerodynamic theory – perfect fluids. In *Aerodynamic Theory II* (ed. W. F. Durand). Dover.

KOOCHESFAHANI, M. M. 1986 Wake of an oscillating airfoil. *Phys. Fluids* **29**, 2776.

KOOCHESFAHANI, M. M. 1989 Vortical patterns in the wake of an oscillating airfoil. *AIAA J.* **27**, 1200–1205.

LARSEN, A. & WALTHER, J. H. 1997 Aeroelastic analysis of bridge girder sections based on discrete vortex simulations. *J. Wind Engng Ind. Aerodyn.* **67–68**, 253–265.

LIGHTHILL, M. J. 1969 Hydromechanics of aquatic animal propulsion. *Annu. Rev. Fluid Mech.* **1**, 413–446.

MACKOWSKI, A. W. & WILLIAMSON, C. H. K. 2015 Direct measurement of thrust and efficiency of an airfoil undergoing pure pitching. *J. Fluid Mech.* **765**, 524–543.

MARAIS, C., THIRIA, B., WESFREID, J. E. & GODOY-DIANA, R. 2012 Stabilizing effect of flexibility in the wake of a flapping foil. *J. Fluid Mech.* **710**, 659–669.

RASMUSSEN, J. T., HEJLESEN, M. M., LARSEN, A. & WALTHER, J. H. 2010 Discrete vortex method simulations of the aerodynamic admittance in bridge aerodynamics. *J. Wind Engng Ind. Aerodyn.* **98**, 754–766.

RIVERA, M., VOROBIEFF, P. & ECKE, R. E. 1998 Turbulence in flowing soap films: velocity, vorticity, and thickness fields. *Phys. Rev. Lett.* **81** (7), 1417–1420.

RUTGERS, M. A., WU, X. L. & DANIEL, W. B. 2001 Conducting fluid dynamics experiments with vertically falling soap films. *Rev. Sci. Instrum.* **72**, 3025–3037.

SCHNIPPER, T., ANDERSEN, A. & BOHR, T. 2009 Vortex wakes of a flapping foil. *J. Fluid Mech.* **644**, 411–423.

SCHNIPPER, T., TOPHØJ, L., ANDERSEN, A. & BOHR, T. 2010 Japanese fan flow. *Phys. Fluids* **22**, 091102.

SFAKIOTAKIS, M., LANE, D. M. & DAVIES, J. B. C. 1999 Review of fish swimming modes for aquatic locomotion. *IEEE J. Ocean. Engng* **24**, 237–252.

TRIANTAFYLLOU, M. S., TRIANTAFYLLOU, G. S. & GOPALKRISHNAN, R. 1991 Wake mechanics for thrust generation in oscillating foils. *Phys. Fluids* A **3**, 2835–2837.

TRIANTAFYLLOU, M. S., TRIANTAFYLLOU, G. S. & YUE, D. K. P. 2000 Hydrodynamics of fishlike swimming. *Annu. Rev. Fluid Mech.* **32**, 33–53.

TYTELL, E. D. & LAUDER, G. V. 2004 The hydrodynamics of eel swimming I. Wake structure. *J. Expl Biol.* **207** (11), 1825–1841.

WALTHER, J. H. & LARSEN, A. 1997 Discrete vortex method for application to bluff body aerodynamics. *J. Wind Engng Ind. Aerodyn.* **67–68**, 183–193.

WILLIAMSON, C. H. K. & ROSHKO, A. 1988 Vortex formation in the wake of an oscillating cylinder. *J. Fluids Struct.* **2**, 335–381.

WU, J. C. 1981 Theory for aerodynamic force and moment in viscous flows. *AIAA J.* **19**, 432–441.

ZHANG, J., CHILDRESS, S., LIBCHABER, A. & SHELLEY, M. 2000 Flexible filaments in a flowing soap film as a model for one-dimensional flags in a two-dimensional wind. *Nature* **408**, 835–839.